First High-Throughput Evaluation of Dark Matter Detector Materials

Sinéad M. Griffin,[1,2] Yonit Hochberg,[3,4] Benjamin V. Lehmann,[5] Rotem Ovadia,[3,4] Kristin A. Persson,[1,6] Bethany A. Suter,[7] Ruo Xi Yang,[1,2] and Wayne Zhao[1,6,8]

[1]*Materials Sciences Division, Lawrence Berkeley National Laboratory, Berkeley, California 94720, USA*
[2]*Molecular Foundry, Lawrence Berkeley National Laboratory, Berkeley, California 94720, USA*
[3]*Racah Institute of Physics, Hebrew University of Jerusalem, Jerusalem 91904, Israel*
[4]*Laboratory for Elementary Particle Physics, Cornell University, Ithaca, New York 14853, USA*
[5]*Center for Theoretical Physics—A Leinweber Institute, Massachusetts Institute of Technology, Cambridge, Massachusetts 02139, USA*
[6]*Department of Materials Science and Engineering, University of California, Berkeley, Berkeley, California 94720 USA*
[7]*Leinweber Institute for Theoretical Physics, University of California, Berkeley, California 94720, USA*
[8]*Liquid Sunlight Alliance and Chemical Sciences Division, Lawrence Berkeley National Laboratory, Berkeley, 94720 California, USA*

(Received 16 July 2025; accepted 18 March 2026; published 11 May 2026)

We perform the first high-throughput search and evaluation of materials that can serve as excellent low-mass dark matter detectors. Using properties of close to 1000 materials from the Materials Project database, we project the sensitivity in dark matter parameter space for experiments constructed from each material, including both absorption and scattering processes between dark matter and electrons. Using the anisotropic materials in the dataset, we further compute the level of daily modulation in interaction rates and the resulting directional sensitivities, highlighting materials with prospects to detect the dark matter wind. Our methods provide the basic tools for the data-driven design of dark matter detectors, and our findings lay the groundwork for the next generation of highly optimized direct searches for dark matter as light as the keV scale. This represents a major step in the application of results from condensed matter physics to dark matter search design.

DOI: 10.1103/bb4g-7939

The identity of the dark matter (DM) in the Universe remains a pressing open question. Decades of experimental searches targeting candidates near the weak scale have yielded null results, which has heightened interest in scenarios with masses well away from the weak scale [1]. Over the last ten years, a robust community effort has emerged to develop experiments capable of probing DM scattering for masses well below a GeV, even down to the keV scale, where cosmological constraints become severe. This program has motivated the study of a wide range of detection modalities and, in particular, various detector constituents. Proposed detector materials range from the familiar to the exotic, including scintillators [2], semiconductors [3–6], superconductors [7–10], superfluid [11,12] and solid helium [13], two-dimensional systems [14,15], aromatic organic compounds [16], and even solid ice [17]. Several of these proposals have already been realized in the laboratory, placing new limits on light DM [8–10,18,19].

Given the vast array of detection strategies with widely varying properties, a key component of this program is the identification of the modalities and materials that will enable the most sensitive experiments. The structure of the detector system, including its constituent materials, determines the nature and properties of the excitations that can be produced by DM interactions. Much of the early work on sub-GeV direct detection focused on identifying systems with detectable low-energy excitations: the detection of light DM is ultimately limited by the energy budget of the incoming DM, which is $\mathcal{O}(\mathrm{meV})$ for elastically scattering keV-scale DM. Designing a system to read out such a small excitation is highly nontrivial. This was, for example, the original motivation for superconductors as DM detectors: since typical superconductors have a gap of $\mathcal{O}(\mathrm{meV})$, they exhibit a set of low-energy excitations suitable for light DM detection.

With experimental technologies now maturing, material selection has come into the limelight. When DM interacts with a detector, the entire detector system can respond to the induced perturbation. The nature of this detector response plays a key role in determining the DM interaction rate at a given energy. Thus, to design an experiment sensitive to light DM, one should aim to optimize the entire

Published by the American Physical Society under the terms of the Creative Commons Attribution 4.0 International license. Further distribution of this work must maintain attribution to the author(s) and the published article's title, journal citation, and DOI. Funded by SCOAP³.

energy- and momentum-dependent detector response in the corresponding regime, which is sensitive to all collective modes of the system. In general, this is a complicated task, since detector response can be difficult to compute. However, for the specific case of spin-independent DM-electron interactions, the role of detector response is now well understood [20–22]. A single "loss function" can be defined in terms of the energy and momentum transfer in the scattering process, and this loss function fully determines the DM interaction rate. Since the loss function in certain regimes also determines the scattering rate of Standard Model particles in the material, it can be measured experimentally or computed using standard tools from the condensed matter community. This opens an opportunity anticipated four years ago by Ref. [20]: that one could rapidly survey a large number of materials for suitability in direct detection experiments.

In this Letter, we realize this analysis for the first time. We use results from the Materials Project (MP) [23–27], a large database of state-of-the-art computations of inorganic material properties, including dielectric response functions, which give rise to the loss function that controls DM interaction rates. This large catalog of computed loss functions allows us to discover candidate materials in a data-driven way, with no prior notion of their properties. (Smaller-scale searches for spin-orbit gapped semiconductors [28] and organic semiconductors [29] have been considered in the context of low-mass DM targets, but these searches focused on computing target properties only and did not evaluate their DM responses. See also Ref. [30] for machine learning of organic target responses.) Moreover, since the MP dataset includes all components of the static dielectric tensor, we can also evaluate the suitability of anisotropic materials for directionally sensitive searches, a crucial step for background rejection in the next generation of experiments [14–16,22,31–41]. Our Letter is the first large-scale application of response functions computed in materials databases and promises to rapidly and dramatically expand the pool of viable DM detector materials by harnessing enormous computational and experimental datasets from beyond the confines of the DM community. Our results have significant and immediate implications for the design of next-generation DM detection experiments, highlighting the power and direct utility of materials science methods for DM science. In this Letter, we use natural units with $c = \hbar = 1$.

DM interaction rate—To calculate the interaction rate between the DM and the electrons in the detector, we follow Refs. [20,22]. We assume that the DM species χ has a spin-independent interaction with electrons in the detector. We denote the energy transferred in the interaction by ω and the 3-momentum transferred by $\mathbf{q}$, with $q = |\mathbf{q}|$. The DM-electron scattering rate is completely determined by the material's loss function $\mathcal{W}(\mathbf{q}, \omega)$, which is related to the longitudinal component of the dielectric tensor ϵ as $\mathcal{W}(\mathbf{q}, \omega) \equiv \mathrm{Im}[-1/(\hat{\mathbf{q}} \cdot \overleftrightarrow{\epsilon}(\mathbf{q}, \omega) \cdot \hat{\mathbf{q}})]$. The underlying premise of this Letter is that dielectric tensors have been computed for many different materials by the MP, and these can be used almost directly to predict the sensitivity of an experiment.

The rate of elastic scattering between DM and an electronic target in the laboratory frame is given in terms of the loss function by

$$R(t) = \frac{1}{\rho_{\mathrm{T}}} \frac{\rho_\chi}{m_\chi} \frac{\pi \bar{\sigma}_{\mathrm{e}}}{\mu_{\mathrm{e}\chi}^2} \int \mathrm{d}^3\mathbf{v}_\chi f_\chi^{\mathrm{lab}}(\mathbf{v}_\chi, t) \times \int \frac{\mathrm{d}^3\mathbf{q}}{(2\pi)^3} \frac{8\pi\alpha}{q^2} \mathcal{F}(q)^2 \mathcal{W}(\mathbf{q}, \omega_{\mathbf{q}}). \quad (1)$$

Here ρ_χ and ρ_{T} are the densities of the DM and the target, respectively; $\mu_{\mathrm{e}\chi}$ is the DM-electron reduced mass; $f_\chi^{\mathrm{lab}}(\mathbf{v}_\chi, t)$ is the DM velocity distribution in the laboratory frame; $\alpha \simeq 1/137$ is the fine structure constant; $\bar{\sigma}_{\mathrm{e}}$ is a reference cross section; $\omega_{\mathbf{q}}(\mathbf{v}_\chi) = \mathbf{v}_\chi \cdot \mathbf{q} - q^2/(2m_\chi)$ is the energy transferred in elastic scattering; $\mathcal{F}(q) \equiv V(q)/V(\alpha m_{\mathrm{e}})$ is a form factor that characterizes the dependence on the mediator, where $V(q) = g_{\mathrm{e}}^2 g_\chi^2/(q^2 + m_\phi^2)$ is the nonrelativistic potential for an interaction mediated by a scalar or vector of mass m_ϕ; and $\bar{\sigma}_{\mathrm{e}} \equiv \mu_{\mathrm{e}\chi}^2 V(\alpha m_{\mathrm{e}})^2/\pi$ is a reference cross section. Note that f_χ^{lab} is time dependent due to the rotation of Earth with respect to its direction of motion through the Galactic halo. The changing direction of the DM "wind" in the laboratory frame translates to a daily modulation in the rate for detectors with anisotropic dielectric tensors [22,42]. This directional sensitivity allows for the detection of the DM wind, enabling strong background rejection and confirmation of a putative discovery [43]. We use the standard halo model [44] for f_χ^{lab}, with dispersion velocity $v_0 = 220$ km/s, escape velocity $v_{\mathrm{esc}} = 550$ km/s, and Earth velocity $v_{\mathrm{E}} = 232$ km/s.

We also consider DM absorption for the case of a kinetically mixed dark photon, i.e., a model with an interaction of the form $\mathcal{L} \supset -\frac{1}{2}\kappa F_{\mu\nu} F'^{\mu\nu}$, where F and F' are the field strength tensors for the Standard Model photon and dark photon, respectively. This interaction will occur at a rate mimicking Standard Model photon absorption in a material, but suppressed by a factor of κ^2. Thus, the absorption rate per unit detector volume per DM particle is given by [5,45]

$$\Gamma_{\mathrm{A}} = \kappa^2 m_\chi \, \mathrm{Im}\left(-\frac{1}{\epsilon(m_\chi \mathbf{v}_\chi, m_\chi)}\right). \quad (2)$$

Since $|\mathbf{v}_\chi| \sim 10^{-3}$, Eq. (2) only samples the loss function in the regime $|\mathbf{q}| \ll \omega$. Thus, when computing the absorption rate, we fix $|\mathbf{q}| = 0$, which gives an excellent approximation for the DM masses considered in this Letter. Here we

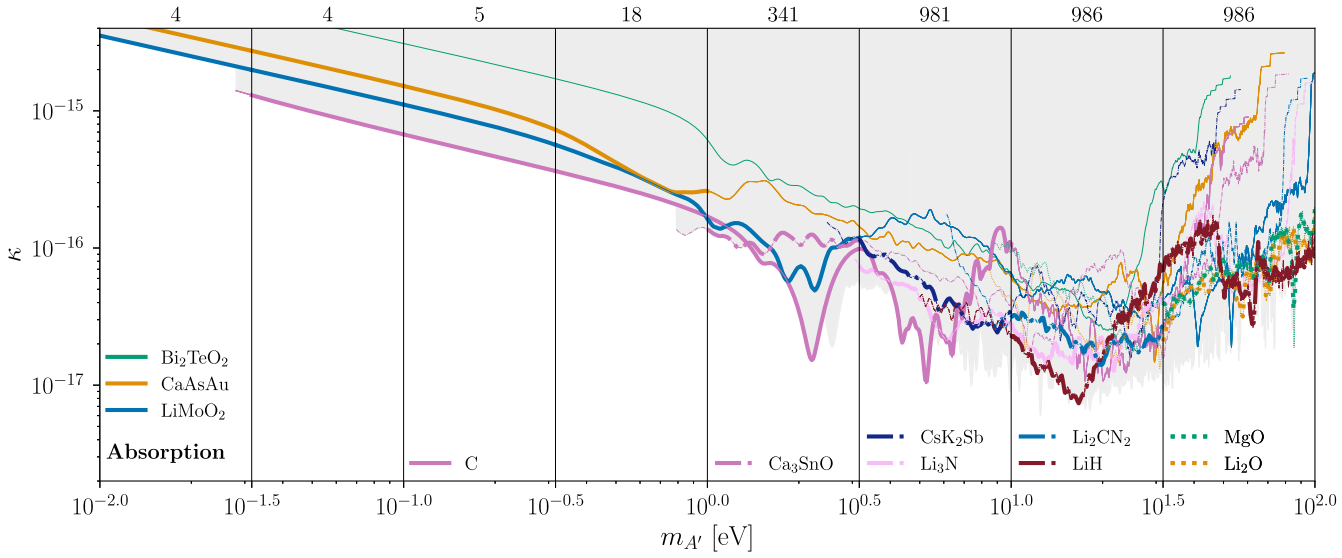

FIG. 1. Absorption. Projected reach of optimal materials from the MP dataset for DM absorption of a kinetically mixed dark photon. In each half-decade of DM mass, materials are ranked by average reach in log space, and the three best from the dataset are indicated by thick lines in each panel. The gray region indicates parameter space that is accessible by the combination of all materials in the MP dataset. The numbers across the top indicate the number of materials with any sensitivity in each mass range. All projections are made at 95% CL for a background-free exposure of 1 kilogram-year.

assume that the dielectric tensor is isotropic and write ϵ in place of $\overleftrightarrow{\epsilon}$. When $\overleftrightarrow{\epsilon}$ is anisotropic, we average over Cartesian directions. The computation of the DM absorption rate in an anisotropic material will be the subject of future work [46].

The MP dataset [23–25] contains dielectric tensors, band gaps, densities, and unit cell volumes. We use improved band gap computations, some of which are not yet incorporated into the MP dataset, and consider 986 out of the original 1019 materials for which reliable band gaps are available. Since the dielectric tensor is provided only in the $\mathbf{q} \to 0$ limit, we extrapolate to finite $\mathbf{q}$ using a custom fitting procedure. A description of the fitting procedure and other dataset details are provided in the End Matter. The full dataset is provided in a public repository released with this Letter [47].

Results and discussion—We can now evaluate the sensitivity of a fiducial experiment to DM scattering and absorption for each of the materials in the MP dataset. For materials with anisotropic dielectric tensors, we further evaluate the amplitude of the daily modulation induced in the scattering rate. The projections are available for all of the materials in our dataset [47], with further details provided in the End Matter.

In order to identify the materials in the dataset with optimal sensitivity for DM searches, one needs a figure of merit for comparison. Given an interval of DM masses (m_1, m_2) and a quantity α characterizing the strength of the weakest detectable interaction for a fixed exposure, we compute the figure of merit $\eta \equiv -\int_{\log m_1}^{\log m_2} \log \alpha(m_\chi) \mathrm{d} \log m_\chi$, so that the largest value of η corresponds to the system that is sensitive to the largest parameter space volume in logarithmic coordinates. For scattering, we take α to be the cross section $\bar{\sigma}_e$ defined in (1), and for absorption, we take α to be the kinetic mixing parameter κ. Ranking materials by the figure of merit η, we can identify the materials with greatest sensitivity in each mass range [48].

Our results for DM absorption of a kinetically mixed dark photon are shown in Fig. 1. In each half-decade of DM mass, we show the projected sensitivity for all materials that are among the three materials with the largest figure of merit in the corresponding bin. The gray shaded region shows the best projected reach across all materials in the MP dataset at each DM mass. All projections are made at the 95% confidence level (CL) assuming a background-free exposure of 1 kg-yr. We consider deposits $\omega > 10$ meV, with the maximal deposit set by the highest energy available in the data for each material, at most 100 eV. We label curves with their chemical formulas for readability, but these formulas do not uniquely determine material properties, since each formula can correspond to many different allotropes. An unambiguous description of a material is provided by its ID in the MP database, or MPID. Table I lists all materials appearing in our plots, including their MPID, relevant band gap, structure type, and whether they have been experimentally synthesized.

Our results for DM scattering are shown in Fig. 2 for the case of a light mediator. The analogous results for a heavy mediator are given in the End Matter (Fig. 4). These are qualitatively similar and select nearly the same set of optimal materials. As with Fig. 1, the lower panel shows the three optimal materials from the MP dataset in each

TABLE I. Materials and their corresponding MPIDs studied in this Letter, listed alphabetically by column. For each material, we report the computed band gap E_g and method: Heyd-Scuseria-Ernzerhof (HSE) hybrid functional (H); r^{2}SCAN meta-generalized gradient approximation (GGA) (r), or GGA (G). We give the structure type for each material and provide a reference when the compound listed has been experimentally synthesized. Materials listed as "Gapless" exhibited vanishing band gaps in each of the available computational methods.

Formula	MPID	E_g (eV)	Structure type	Formula	MPID	E_g (eV)	Structure type
Bi_2TeO_2	mp-755419 [49]	Gapless	Anti-$ThCr_2Si_2$ [50]	KNa_2Bi	mp-863707 [51]	0.43 (H)	DO_3 type [52]
C	mp-569304 [53]	0.21 (r)	AABBCC graphite [54]	$LaBr_2$	mp-28572 [55]	1.00 (H)	$2H_2$-MoS_2 [56]
Ca_3SnO	mp-29241 [57]	0.40 (H)	Inverse perovskite [58]	Li_2CN_2	mp-9610 [59]	4.93 (H)	Tetragonal $I4/mmm$ [60]
CaAsAu	mp-3927 [61]	Gapless	Hexagonal ω [62]	Li_2O	mp-1960 [63]	6.66 (H)	CaF_2 (fluorite) [64]
$CaCdO_2$	mp-753287 [65]	1.12 (r)	Caswellsilverite-like	Li_3N	mp-2251 [66]	2.03 (H)	Layered $P6/mmm$ [67]
$CoAuO_2$	mp-997161 [68]	0.63 (r)	$CuFeO_2$ (delafossite)	LiH	mp-23703 [69]	3.99 (H)	NaCl (rocksalt) [70]
Cs_2O	mp-7988 [71]	1.34 (r)	Anti-CdC_{l2}/layer [72]	$LiMoO_2$	mp-19338 [73]	Gapless	Layered caswellsilverite [74]
CsK_2Sb	mp-581024 [75]	1.67 (H)	M_3Sb (M:alkali metal) [76]	MgO	mp-1265 [77]	6.62 (H)	NaCl (rocksalt) [78]
K_2PdBr_6	mp-1205761 [79]	1.29 (H)	K_2PtCl_6 [80]	SrAlSiH	mp-570485 [81]	0.63 (G)	Layered Zintl hydride [82]
$KCuTeO_6$	mp-1147551 [83]	2.0 (H)	Layered				

half-decade of DM mass. The top panel shows optimal materials for the directional detection of the DM wind. For a fixed exposure, this "anisotropic reach" is defined by the cross section for which the null hypothesis of an isotropic DM distribution can be rejected at 95% CL. The anisotropic reach always corresponds to larger cross sections, since many events are required to establish that the arrival directions are not uniformly distributed. The anisotropic

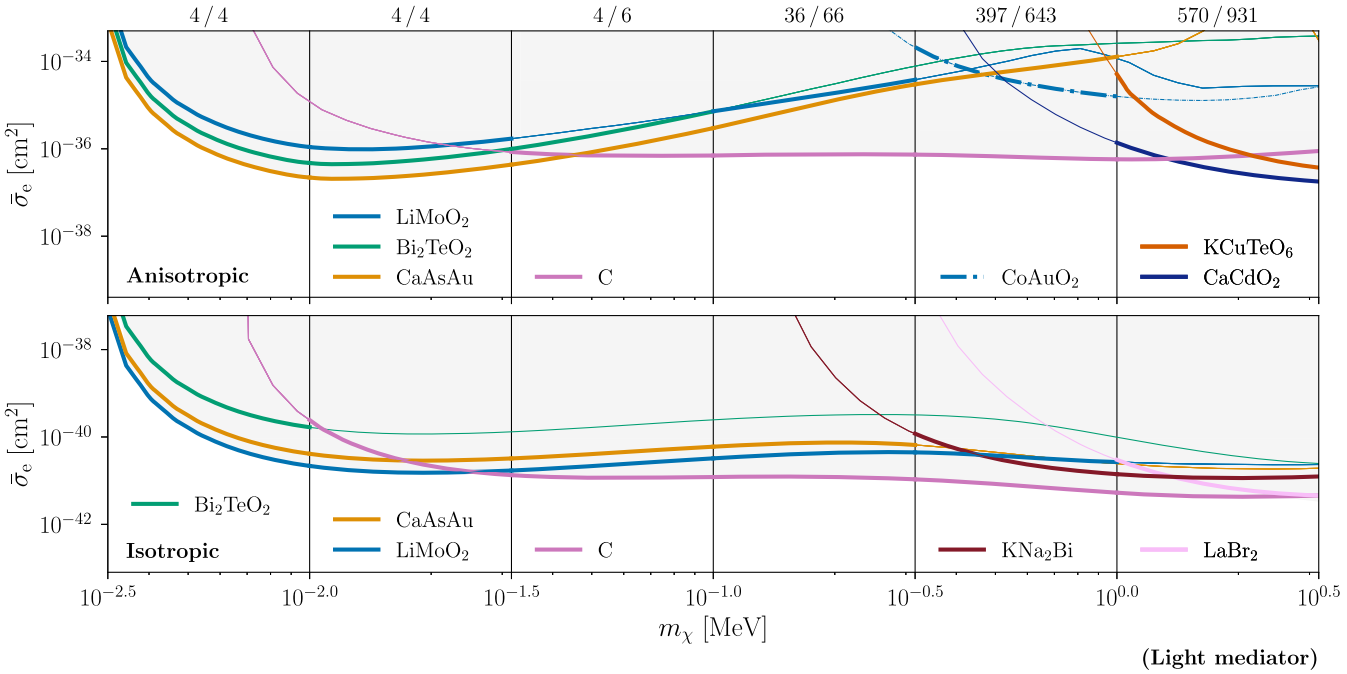

FIG. 2. Scattering via a light mediator. Projected reach of optimal materials in the MP dataset for DM scattering via a light mediator, selected on the same criteria as in Fig. 1. Bottom: optimal materials in the MP dataset on the basis of 3 event reach. Top: optimal materials on the basis of sensitivity to anisotropy in the DM distribution. The pairs of numbers across the top indicate the number of materials with any sensitivity in each mass range: the first and second numbers correspond to anisotropic and isotropic sensitivity, respectively. All projections are made at 95% CL for a kilogram-year of exposure.

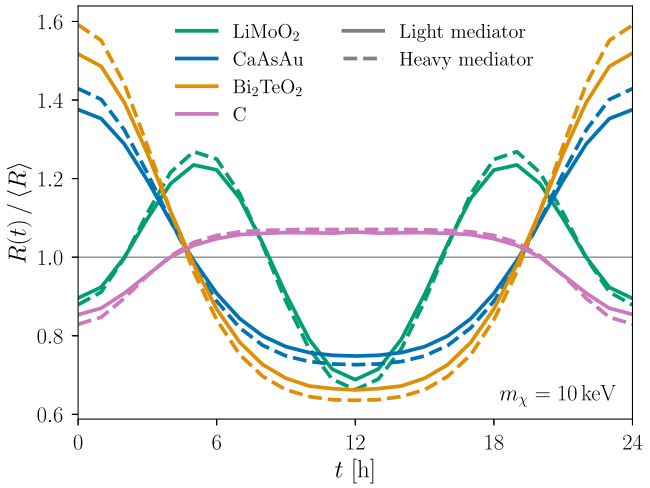

FIG. 3. Daily modulation of the DM scattering rate for four selected materials calculated for $m_\chi = 10$ keV. Solid (dashed) lines correspond to a light (heavy) mediator. The materials $CaCdO_2$, $CoAuO_2$, and $KCuTeO_6$ exhibit daily modulations of similar order at $m_\chi \sim$ MeV.

reach is representative of the best possible sensitivity in the presence of uncontrolled backgrounds, where the detection of the DM wind direction is crucial in order to distinguish the DM signal from other sources.

A key difference between our results for absorption and scattering is the range of masses over which particular materials are optimal. The kinematics of DM absorption involves an energy transfer on the order of the DM mass, which is much larger than the momentum transfer. Accordingly, localized features of the response function result in localized features in the reach curve, so a material that is optimal in one half-decade of mass is not generically optimal elsewhere. On the other hand, the kinematics of scattering average the response over a range of energy transfers, leading to smoother reach curves and to materials that are optimal over wide mass ranges.

One might hope to optimize DM searches by selecting materials that offer excellent reach for both absorption and scattering simultaneously, and for the widest possible mass range. A small number of materials are among the optimal three across multiple half-decades of DM mass. For absorption, these materials are C, $LiMoO_2$, and Li_3N. For isotropic scattering, these materials are C, $LiMoO_2$, CaAsAu, and KNa_2Bi. For anisotropic scattering, these are C, $LiMoO_2$, CaAsAu, Bi_2TeO_2, and $CaCdO_2$. We show the modulation in the DM scattering rate over 24 h for some of these materials in Fig. 3.

Three materials are of particular interest: $LiMoO_2$, CaAsAu, and Bi_2TeO_2 offer strong performance for each of absorption, isotropic scattering, and anisotropic scattering at the lowest DM masses, with daily modulations of $\mathcal{O}(20\% - 50\%)$. $LiMoO_2$ (lithium molybdenate) is well known [84–86] and has been shown to intercalate Li. Bi_2TeO_2, a bismuth oxychalcogenide, is known as a thermoelectric material. It has been studied theoretically by Ref. [87] and is commercially available. CaAsAu, while not widely studied, has been synthesized [62], and Ref. [88] identifies it as a topological semimetal. (Note that the flag "predicted stable" on the MP is one of several descriptors of synthesizability and does not necessarily indicate that a material can or cannot be synthesized.) Our results motivate experimental evaluation of these materials as targets for DM searches. Detailed density functional theory (DFT) computations of their loss functions at nonvanishing momenta will also be pursued in future work [89].

While several detector materials have thus far been evaluated or calibrated with dielectric response data, the materials that we have identified as optimal within our dataset are unique in that they are the first to have been selected by data-driven techniques. Our Letter constitutes the first high-throughput search and evaluation of DM responses in materials datasets for DM detector materials and represents the natural next step in the use of material data for DM experiments. Thus, our method has enabled the evaluation of a large number of heterogeneous candidates, rather than a handful of hand-picked materials. The anisotropies that we project are especially notable: in recent years, directional sensitivity has typically been identified as a rare feature of very specific and highly unusual systems, discovered through great manual effort, to the extent that each individual system warranted a dedicated publication. By contrast, in this Letter, we have identified a large number of robustly direction-sensitive materials that can be used in DM experiments, a complete change of paradigm. We stress that now that large volumes of data are available, the data-driven approach can be used not only for detector calibration, but also for material discovery. As the Materials Project and other large-scale efforts continue to expand their datasets, the DM direct detection community will have the immediate opportunity to identify new classes of materials to accelerate DM detection well below the GeV scale.

The color palette for figures in this Letter was selected programmatically [90] to minimize overlap for several types of color vision deficiency using the color model of Ref. [92].

Acknowledgments—We thank Roni Ilan, Zohar Ringel, and Bashi Mandava for useful discussions and Dino Novko and Antonio Politano for valuable input. We thank Aaron D. Kaplan for contributions to the computation of HSE band gaps used in this work. We thank Leor and Maya Kuflik for valuable comments on color selection. S. M. G., K. A. P., and R. Y. acknowledge support from the U.S. Department of Energy, Office of Science, Office of Basic Energy Sciences, Materials Sciences and Engineering Division under Contract No. DE-AC02-05CH11231 (Materials Project Program No. KC23MP). Work at the Molecular Foundry was supported by the Office of Science, Office of Basic Energy Sciences, of the U.S. Department of

Energy under Contract No. DE-AC02-05CH11231. Computational resources were provided by the National Energy Research Scientific Computing Center, DOE Office of Science User Facilities supported by the Office of Science, U.S. Department of Energy under the same contract number. The work of Y. H. is supported in part by the Israel Science Foundation (Grant No. 1818/22) and by the Binational Science Foundation (Grants No. 2018140 and No. 2022287). The work of Y. H. and R. O. is supported by an ERC STG grant ("Light-Dark," Grant No. 101040019). The work of R. O. is further supported by the Azrieli Fellowship, the Milner Fellowship and the Binational Science Foundation Travel Grant No. 308300002, and the gracious hospitality of Cornell University. The work of B. V. L. is supported by the MIT Pappalardo Fellowship. The work of B. A. S. is supported by the NSF GRFP Fellowship and BSF-2018140. W. Z. acknowledges support from the Liquid Sunlight Alliance, which is supported by the U.S. Department of Energy, Office of Science, Office of Basic Energy Sciences, Fuels from Sunlight Hub under the Award No. DE-SC0021266. This project has received funding from the European Research Council (ERC) under the European Union's Horizon Europe research and innovation program (Grant Agreement No. 101040019). This material is based upon work supported by the National Science Foundation Graduate Research Fellowship Program under Grant No. DGE 2146752.

Views and opinions expressed are those of the author(s) only and do not necessarily reflect those of the European Union. The European Union cannot be held responsible for them. Any opinions, findings, and conclusions or recommendations expressed in this material are those of the author(s) and do not necessarily reflect the views of the National Science Foundation.

Data availability—The data that support the findings of this article are openly available [47].

[1] R. Essig, J. Mardon, and T. Volansky, Phys. Rev. D **85**, 076007 (2012).
[2] S. Derenzo, R. Essig, A. Massari, A. Soto, and T.-T. Yu, Phys. Rev. D **96**, 016026 (2017).
[3] R. Essig, M. Fernandez-Serra, J. Mardon, A. Soto, T. Volansky, and T.-T. Yu, J. High Energy Phys. 05 (2016) 046.
[4] P. W. Graham, D. E. Kaplan, S. Rajendran, and M. T. Walters, Phys. Dark Universe **1**, 32 (2012).
[5] Y. Hochberg, T. Lin, and K. M. Zurek, Phys. Rev. D **95**, 023013 (2017).
[6] S. M. Griffin, Y. Hochberg, K. Inzani, N. Kurinsky, T. Lin, and T. C. Yu, Phys. Rev. D **103**, 075002 (2021).
[7] Y. Hochberg, Y. Zhao, and K. M. Zurek, Phys. Rev. Lett. **116**, 011301 (2016).
[8] Y. Hochberg, I. Charaev, S.-W. Nam, V. Verma, M. Colangelo, and K. K. Berggren, Phys. Rev. Lett. **123**, 151802 (2019).
[9] Y. Hochberg, B. V. Lehmann, I. Charaev, J. Chiles, M. Colangelo, S. W. Nam, and K. K. Berggren, Phys. Rev. D **106**, 112005 (2022).
[10] J. Gao, Y. Hochberg, B. V. Lehmann, S. W. Nam, P. Szypryt, M. R. Vissers, and T. Xu, arXiv:2403.19739.
[11] K. Schutz and K. M. Zurek, Phys. Rev. Lett. **117**, 121302 (2016).
[12] S. Knapen, T. Lin, and K. M. Zurek, Phys. Rev. D **95**, 056019 (2017).
[13] O. A. Ashour and S. M. Griffin, arXiv:2409.02439.
[14] Y. Hochberg, Y. Kahn, M. Lisanti, C. G. Tully, and K. M. Zurek, Phys. Lett. B **772**, 239 (2017).
[15] G. Cavoto, F. Luchetta, and A. D. Polosa, Phys. Lett. B **776**, 338 (2018).
[16] C. Blanco, Y. Kahn, B. Lillard, and S. D. McDermott, Phys. Rev. D **104**, 036011 (2021).
[17] N. Taufertshöfer, M. Garcia-Sciveres, and S. M. Griffin, Phys. Rev. D **110**, 103552 (2024).
[18] P. Adari *et al.* (SENSEI Collaboration), Phys. Rev. Lett. **134**, 011804 (2025).
[19] M. F. Albakry *et al.* (SuperCDMS Collaboration), Phys. Rev. D **111**, 012006 (2025).
[20] Y. Hochberg, Y. Kahn, N. Kurinsky, B. V. Lehmann, T. C. Yu, and K. K. Berggren, Phys. Rev. Lett. **127**, 151802 (2021).
[21] S. Knapen, J. Kozaczuk, and T. Lin, Phys. Rev. D **104**, 015031 (2021).
[22] C. Boyd, Y. Hochberg, Y. Kahn, E. D. Kramer, N. Kurinsky, B. V. Lehmann, and T. C. Yu, Phys. Rev. D **108**, 015015 (2023).
[23] A. Jain *et al.*, APL Mater. **1**, 011002 (2013).
[24] I. Petousis, D. Mrdjenovich, E. Ballouz, M. Liu, D. Winston, W. Chen, T. Graf, T. D. Schladt, K. A. Persson, and F. B. Prinz, Sci. Data **4**, 160134 (2017).
[25] R. X. Yang, M. K. Horton, J. Munro, and K. A. Persson, arXiv:2209.02918.
[26] M. K. Horton *et al.*, Nat. Mater. **24**, 1522 (2025).
[27] Publicly available at https://next-gen.materialsproject.org/.
[28] K. Inzani, A. Faghaninia, and S. M. Griffin, Phys. Rev. Res. **3**, 013069 (2021).
[29] R. M. Geilhufe, B. Olsthoorn, A. Ferella, T. Koski, F. Kahlhoefer, J. Conrad, and A. V. Balatsky, Phys. Status Solidi RRL **12**, 1800293 (2018).
[30] C. Cook, C. Blanco, and J. Smirnov, Phys. Rev. D **112**, 083005 (2025).
[31] Y. Hochberg, Y. Kahn, M. Lisanti, K. M. Zurek, A. G. Grushin, R. Ilan, S. M. Griffin, Z.-F. Liu, S. F. Weber, and J. B. Neaton, Phys. Rev. D **97**, 015004 (2018).
[32] R. Budnik, O. Chesnovsky, O. Slone, and T. Volansky, Phys. Lett. B **782**, 242 (2018).
[33] F. Kadribasic, N. Mirabolfathi, K. Nordlund, A. E. Sand, E. Holmström, and F. Djurabekova, Phys. Rev. Lett. **120**, 111301 (2018).
[34] S. Griffin, S. Knapen, T. Lin, and K. M. Zurek, Phys. Rev. D **98**, 115034 (2018).
[35] M. Heikinheimo, K. Nordlund, K. Tuominen, and N. Mirabolfathi, Phys. Rev. D **99**, 103018 (2019).

[36] A. Coskuner, A. Mitridate, A. Olivares, and K. M. Zurek, Phys. Rev. D **103**, 016006 (2021).
[37] R. M. Geilhufe, F. Kahlhoefer, and M. W. Winkler, Phys. Rev. D **101**, 055005 (2020).
[38] A. Coskuner, T. Trickle, Z. Zhang, and K. M. Zurek, Phys. Rev. D **105**, 015010 (2022).
[39] S. Sassi, A. Dinmohammadi, M. Heikinheimo, N. Mirabolfathi, K. Nordlund, H. Safari, and K. Tuominen, Phys. Rev. D **104**, 063037 (2021).
[40] Y. Hochberg, E. D. Kramer, N. Kurinsky, and B. V. Lehmann, Phys. Rev. D **107**, 076015 (2023).
[41] C. Blanco, I. Harris, Y. Kahn, B. Lillard, and J. Pérez-Ríos, Phys. Rev. D **106**, 115015 (2022).
[42] D. N. Spergel, Phys. Rev. D **37**, 1353 (1988).
[43] F. Mayet *et al.*, Phys. Rep. **627**, 1 (2016).
[44] J. D. Lewin and P. F. Smith, Astropart. Phys. **6**, 87 (1996).
[45] S. Knapen, J. Kozaczuk, and T. Lin, Phys. Rev. D **105**, 015014 (2022).
[46] B. V. Lehmann *et al.* (to be published).
[47] S. M. Griffin, Y. Hochberg, B. V. Lehmann, R. Ovadia, K. A. Persson, B. A. Suter, R. X. Yang, and W. Zhao, Zenodo, 10.5281/zenodo.13346342 (2025).
[48] Note that only a small portion of the full MP database includes dielectric responses so far, so we describe materials as "optimal" only insofar as they are the best performers in the current dataset. Indeed, other materials not included in our dataset are known to exhibit better isotropic sensitivity in some mass ranges. Future application of our pipeline to improved versions of the dataset may reveal materials with better sensitivity as the dataset evolves.
[49] https://next-gen.materialsproject.org/materials/mp-755419.
[50] S. D. N. Luu and P. Vaqueiro, J. Solid State Chem. France **226**, 219 (2015).
[51] https://next-gen.materialsproject.org/materials/mp-863707.
[52] D. E. Sands, D. H. Woods, and W. J. Ramsey, Acta Crystallogr. **16**, 316 (1963).
[53] https://next-gen.materialsproject.org/materials/mp-569304.
[54] D. E. Nixon, G. S. Parry, and A. R. Ubbelohde, Proc. R. Soc. A **291**, 324 (1966).
[55] https://next-gen.materialsproject.org/materials/mp-28572.
[56] K. Krämer, T. Schleid, M. Schulze, W. Urland, and G. Meyer, Z. Anorg. Allg. Chem. **575**, 61 (1989).
[57] https://next-gen.materialsproject.org/materials/mp-29241.
[58] A. Widera and H. Schäfer, Mater. Res. Bull. **15**, 1805 (1980).
[59] https://next-gen.materialsproject.org/materials/mp-9610.
[60] M. G. Down, M. J. Haley, P. Hubberstey, R. J. Pulham, and A. E. Thunder, J. Chem. Soc. Dalton Trans. **10**, 1407 (1978).
[61] https://next-gen.materialsproject.org/materials/mp-3927.
[62] D. Johrendt, R. Miericke, and A. Mewis, Z. Naturforsch. B **51**, 905 (1996).
[63] https://next-gen.materialsproject.org/materials/mp-1960.
[64] J. Bijvoet, A. Claassen, and A. Karssen, in *Proceedings of the Koninklijke Nederlandse Academie van Wetenschappen* (1926), Vol. 29, pp. 1286–1292.
[65] https://next-gen.materialsproject.org/materials/mp-753287.
[66] https://next-gen.materialsproject.org/materials/mp-2251.
[67] A. Rabenau and H. Schulz, J. Less Common Metals **50**, 155 (1976).
[68] https://next-gen.materialsproject.org/materials/mp-997161.
[69] https://next-gen.materialsproject.org/materials/mp-23703.
[70] W. B. Zimmerman, Phys. Rev. B **5**, 4704 (1972).
[71] https://next-gen.materialsproject.org/materials/mp-7988.
[72] K.-R. Tsai, P. M. Harris, and E. N. Lassettre, J. Phys. Chem. **60**, 338 (1956).
[73] https://next-gen.materialsproject.org/materials/mp-19338.
[74] L. E. Aleandri and R. E. McCarley, Inorg. Chem. **27**, 1041 (1988).
[75] https://next-gen.materialsproject.org/materials/mp-581024.
[76] W. McCarroll, J. Phys. Chem. Solids **26**, 191 (1965).
[77] https://next-gen.materialsproject.org/materials/mp-1265.
[78] E. Broch, Z. Phys. Chem. **127**, 446 (1927).
[79] https://next-gen.materialsproject.org/materials/mp-1205761.
[80] J. A. A. Ketblaar and J. F. van Walsem, Recl. Trav. Chim. Pays-Bas **57**, 964 (1938).
[81] https://next-gen.materialsproject.org/materials/mp-570485.
[82] M. H. Lee, T. Björling, B. C. Hauback, T. Utsumi, D. Moser, D. Bull, D. Noréus, O. F. Sankey, and U. Häussermann, Phys. Rev. B **78**, 195209 (2008).
[83] https://next-gen.materialsproject.org/materials/mp-1147551.
[84] J. Barker, M. Y. Saidi, and J. L. Swoyer, Electrochem. Solid-State Lett. **6**, A252 (2003).
[85] J. Barker, M. Saidi, and J. Swoyer, Solid State Ionics **158**, 261 (2003).
[86] K. Ben-Kamel, N. Amdouni, H. Groult, A. Mauger, K. Zaghib, and C. Julien, J. Power Sources **202**, 314 (2012).
[87] J. M. Flitcroft, A. Althubiani, and J. M. Skelton, J. Phys. Energy **6**, 025011 (2024).
[88] T. Zhang, Y. Jiang, Z. Song, H. Huang, Y. He, Z. Fang, H. Weng, and C. Fang, Nature (London) **566**, 475 (2019).
[89] Y. Hochberg, B. V. Lehmann *et al.* (to be published).
[90] Recently, we developed a package, MonteColor [91], for creating custom colorblind-safe palettes. MonteColor is publicly available at https://github.com/benvlehmann/montecolor.
[91] Benjamin V. Lehmann, MonteColor (2025), http://github.com/benvlehmann/montecolor.
[92] M. R. Luo, G. Cui, and C. Li, Color Res. Appl. **31**, 320 (2006).
[93] We use the full anisotropic dielectric tensor for the purposes of estimating rate modulations, as described in the next subsection. The degree of anisotropy has minimal impact on the average rate.
[94] M. Dressel and G. Grüner, *Electrodynamics of Solids: Optical Properties of Electrons in Matter* (Cambridge University Press, Cambridge, England, 2002).
[95] I. Abril, R. Garcia-Molina, C. D. Denton, F. J. Pérez-Pérez, and N. R. Arista, Phys. Rev. A **58**, 357 (1998).
[96] M. Vos and P. L. Grande, J. Phys. Chem. Solids **124**, 242 (2019).
[97] Y. Hochberg, D. Novko, R. Ovadia, and A. Politano, arXiv:2507.07164.
[98] See Supplemental Material at http://link.aps.org/supplemental/10.1103/bb4g-7939 for additional information about the dataset, further details of our fitting procedure, and benchmarks for the fitted dielectric functions, which includes Refs. [99–106].

[99] J. P. Perdew, K. Burke, and M. Ernzerhof, Phys. Rev. Lett. **77**, 3865 (1996).
[100] R. Kingsbury, A. S. Gupta, C. J. Bartel, J. M. Munro, S. Dwaraknath, M. Horton, and K. A. Persson, Phys. Rev. Mater. **6**, 013801 (2022).
[101] J. W. Furness, A. D. Kaplan, J. Ning, J. P. Perdew, and J. Sun, J. Phys. Chem. Lett. **11**, 8208 (2020).
[102] J. Heyd, G. E. Scuseria, and M. Ernzerhof, J. Chem. Phys. **118**, 8207 (2003).
[103] A. V. Krukau, O. A. Vydrov, A. F. Izmaylov, and G. E. Scuseria, J. Chem. Phys. **125**, 224106 (2006).
[104] W. Zhao, R. X. Yang, A. D. Kaplan, and K. A. Persson, ACS Materials Au, 10.1021/acsmaterialsau.5c00100 (2025).
[105] S. Carrazza and J. M. Cruz-Martinez, Comput. Phys. Commun. **254**, 107376 (2020).
[106] S. Carrazza and J. M. Cruz-Martinez, N3pdf/VEGASFLOW: VEGASFLOW v1.0 (2020).
[107] L. Barak *et al.* (SENSEI Collaboration), Phys. Rev. Lett. **125**, 171802 (2020).
[108] D. Amaral *et al.* (SuperCDMS Collaboration), Phys. Rev. D **102**, 091101 (2020).
[109] A. Aguilar-Arevalo *et al.* (DAMIC Collaboration), Phys. Rev. Lett. **123**, 181802 (2019).
[110] R. Essig, T. Volansky, and T.-T. Yu, Phys. Rev. D **96**, 043017 (2017).
[111] P. Agnes *et al.* (DarkSide Collaboration), Phys. Rev. Lett. **121**, 111303 (2018).
[112] E. Aprile *et al.* (XENON Collaboration), Phys. Rev. Lett. **123**, 251801 (2019).

End Matter

Dataset and fitting procedure—In the MP dataset, the dielectric tensor $\overleftrightarrow{\epsilon}_{\rm data}$ is only available in the limit $\mathbf{q} \to 0$. This is sufficient to treat DM absorption, which always takes place in the small-q limit, but it is insufficient for DM scattering. It is therefore necessary to adopt a fixed procedure for estimating the dielectric tensor at $q > 0$. We use the following steps. First, if $\overleftrightarrow{\epsilon}_{\rm data}$ is anisotropic, we average $\hat{\mathbf{q}} \cdot \overleftrightarrow{\epsilon}_{\rm data} \cdot \hat{\mathbf{q}}$ over Cartesian directions to obtain a scalar dielectric function $\epsilon_{\rm data}$ for the purposes of estimating the overall rate [93]. Next, we extract all energies $\hat{\omega}_k$ where $\mathrm{Re}(\epsilon)$ vanishes. Each of these zeros except the first, $\hat{\omega}_0$, corresponds to a plasmon peak in the loss function. We fit each of these peaks with a Lindhard dielectric function $\epsilon_{\rm L}$ [94], fixing the plasma frequency to $\omega_{{\rm p},k} = \hat{\omega}_k$ and fitting the plasmon width $\Gamma_{{\rm p},k}$. We then construct a q-dependent loss function as the linear combination of these fits,

$$\mathcal{W}_{\rm fit}(\mathbf{q},\omega) = \frac{1}{\sum_k h_k} \sum_{k=1}^{n_{\rm peaks}} h_k \,\mathrm{Im}\left(-\frac{1}{\epsilon_{\rm L}(\omega_{{\rm p},k}, \Gamma_{{\rm p},k}; \mathbf{q}, \omega)}\right). \tag{A1}$$

(Sums of model loss functions have been previously used to approximate losses in real materials, e.g., by Refs. [95,96].) This does not reduce to the loss function constructed from $\epsilon_{\rm data}$ as $q \to 0$. Thus, when defining the q-dependent loss function, we incorporate the residual ratio between the data and the fit to enforce agreement at $q = 0$, and we make the approximation that this ratio is independent of q. Specifically, we define $r(\omega) \equiv \mathrm{Im}[-1/\epsilon_{\rm data}(\omega)]/\mathcal{W}_{\rm fit}(\mathbf{q},\omega)|_{\mathbf{q}\to 0}$ and use a modified loss function

$$\mathcal{W}_r(\mathbf{q},\omega) = r(\omega) \times \mathcal{W}_{\rm fit}(\mathbf{q},\omega), \tag{A2}$$

which retains the momentum dependence implied by the fitted Lindhard functions, but is constructed to yield $\mathcal{W}_{\rm data}$ in the limit $q \to 0$. We use $\mathcal{W}_r$ as a proxy for the material's loss function at $q > 0$ in our rate computations. While this empirical fitting procedure does not arise from a microphysical model, it is nonetheless capable of reproducing results from dedicated DFT computations in other materials [97]. Finally, we conservatively fix $\mathcal{W}_{\rm fit}(\mathbf{q},\omega) = 0$ for values of ω below the gap in the material. We exclude 55 materials due to incompatibility with our fitting procedure, all with band gaps above 1 eV. We thus evaluate a total of 931 materials for isotropic scattering sensitivity.

To calculate the daily modulation of the DM scattering rate induced by the rotation of Earth, we use a directionally-dependent generalization of the fitting procedure described above: we separately fit $\hat{\mathbf{q}} \cdot \overleftrightarrow{\epsilon}_{\rm data} \cdot \hat{\mathbf{q}}$ for 800 uniformly sampled directions $\hat{\mathbf{q}}_i$, with the plasmon parameters and ratio factors $r(\omega)$ computed independently from the longitudinal dielectric tensor along each direction. We perform this directionally-dependent fit for materials in which the loss function differs by at least 25% on average between two Cartesian axes. Of the 931 materials evaluated for scattering sensitivity, 593 exhibit this level of anisotropy. To avoid sensitivity to artificial anisotropy introduced by the fitting procedure, we check for the presence of approximate uniaxial symmetry in any of the material axes and find such a symmetry in 527 of the anisotropic materials. For these materials, we enforce the rotational symmetry by averaging the components of $\overleftrightarrow{\epsilon}_{\rm data}$ around the symmetry axis prior to fitting. Of the 593 anisotropic materials, 23 were incompatible with our fitting procedure and were excluded, all with band gaps above 1 eV. We compute the modulation following Ref. [22], and when evaluating $\mathcal{W}_{\rm fit}(\mathbf{q})$, we use the fit in the direction $\hat{\mathbf{q}}_i$ closest to $\hat{\mathbf{q}}$. Uniaxial materials are oriented with their axis perpendicular to the DM wind. For other materials, one of the Cartesian axes is oriented in this way, chosen to maximize the modulation. Further details of the selection criteria, preprocessing steps, and statistical analysis are given in Supplemental Material [98].

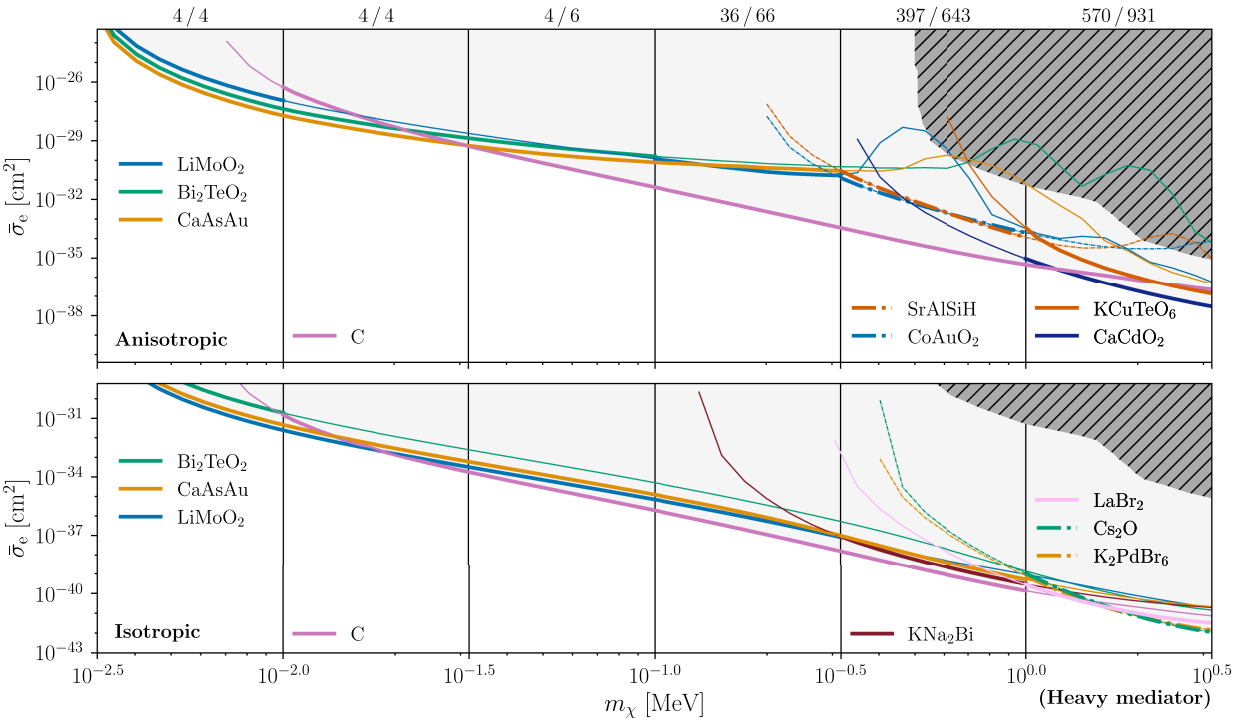

FIG. 4. Scattering via heavy mediator. Projected reach of optimal materials for DM scattering via a heavy mediator. Existing constraints from Refs. [107–112] are indicated by the hatched dark gray region. All other features are identical to Fig. 2.

Additional results and public repository—In the main text, we show reach curves for absorption and for scattering via a light mediator, each for a small subset of materials that are optimal in the MP dataset according to our criteria. Here, we supply results for the two remaining cases: scattering via a heavy mediator and scattering or absorption with all of the other materials in our dataset.

First, we present our results for DM scattering via a heavy mediator in Fig. 4. The hatched region in Fig. 4 indicates existing constraints on the relevant parameter space. As mentioned in the main text, the qualitative outcome of this analysis is very similar to the case of the light mediator that we show in Fig. 2. The full set of optimal materials is very similar between the two cases.

Next, for all the cases for which projections appear in this Letter, and for all other materials in the Materials Project dataset, we have made our data products publicly available [47] to facilitate future studies. For each material in our dataset, the repository includes the following properties: (1) The full dielectric tensor data in the limit $q \to 0$; (2) other material data such as band gaps and densities; (3) projected reach curves for absorption, isotropic scattering, and anisotropic scattering; (4) modulation curves for anisotropic materials, error estimates, and planar symmetries.

Dielectric response data in the repository are shifted per the procedure described in Supplemental Material [98]. Further documentation and usage examples are included in the repository itself.